Acta Oceanol. Sin., 2017, Vol. 36, No. 11, P. 38–50
DOI: 10.1007/s13131-017-1073-4
http://www.hyxb.org.cn
E-mail: hyxbe@263.net

Revisiting the seasonal wave height variability in the South China Sea with merged satellite altimetry observations

SU Hui[1], WEI Chunlei[2], JIANG Shaocai[2], LI Peiliang[3], ZHAI Fangguo[3]*

[1] Central Marine Environmental Monitoring Station of Xiamen, East China Sea Branch, State Oceanic Administration, Xiamen 361008, China

[2] Beihai Marine Environmental Monitoring Center, South China Sea Branch, State Oceanic Administration, Beihai 536007, China

[3] College of Oceanic and Atmospheric Sciences, Ocean University of China, Qingdao 266100, China

Received 22 March 2016; accepted 25 August 2016

Abstract

The seasonal variability of the significant wave height (SWH) in the South China Sea (SCS) is investigated using the most up-to-date gridded daily altimeter data for the period of September 2009 to August 2015. The results indicate that the SWH shows a uniform seasonal variation in the whole SCS, with its maxima occurring in December/January and minima in May. Throughout the year, the SWH in the SCS is the largest around Luzon Strait (LS) and then gradually decreases southward across the basin. The surface wind speed has a similar seasonal variation, but with different spatial distributions in most months of the year. Further analysis indicates that the observed SWH variations are dominated by swell. The wind sea height, however, is much smaller. It is the the largest in two regions southwest of Taiwan Island and southeast of Vietnam Coast during the northeasterly monsoon, while the largest in the central/southern SCS during the southwesterly monsoon. The extreme wave condition also experiences a significant seasonal variation. In most regions of the northern and central SCS, the maxima of the 99th percentile SWH that are larger than the SWH theoretically calculated with the wind speed for the fully developed seas mainly appear in August–November, closely related to strong tropical cyclone activities. Compared with previous studies, it is also implied that the wave climate in the Pacific Ocean plays an important role in the wave climate variations in the SCS.

Key words: significant wave height, seasonal variability, South China Sea, satellite observations

Citation: Su Hui, Wei Chunlei, Jiang Shaocai, Li Peiliang, Zhai Fangguo. 2017. Revisiting the seasonal wave height variability in the South China Sea with merged satellite altimetry observations. Acta Oceanologica Sinica, 36(11): 38–50, doi: 10.1007/s13131-017-1073-4

1 Introduction

The South China Sea (SCS) is the largest semi-enclosed sea in the western tropical Pacific Ocean, and has a large northeast-southwest oriented abyssal basin (e.g., Liu et al., 2008). It is crucial to elucidate changes in the wave climate of the SCS in the design and operation of offshore industries, the selection of ship routing, the assessment of the wave energy, and the risk assessment of the future vulnerability to possible coastal disasters. In the literature, the wave climate in the SCS has attracted many attentions, which mainly focus on its variations on seasonal, interannual and decadal time scales, and also its long term trends (e.g., Yu, 1984; Chen, 1987; Chen et al., 2006; Qi et al., 1997; Qi and Shi, 1999; Zhou et al., 2007; Guo et al., 2012; Li et al., 2012; Zheng et al., 2014; Zong and Wu, 2014; Wan et al., 2015; Zhu et al., 2015).

On the basis of TOPEX satellite altimetry observations from December 1992 to March 2005, Chen et al. (2006) found that in the SCS the temporal variations of the significant wave height (SWH) were dominated by the seasonal variation. They argued that the seasonal mean SWH was the largest in winter, while the smallest in summer. This result is roughly consistent with the observations obtained by GEOSAT satellite (Qi et al., 1997) and numerical simulations (e.g., Zhou et al., 2007). On the other hand, however, there are also many other studies proving that the SWH is the weakest in spring (mainly in April and May) using ship observations, satellite observations, and also numerical simulations (e.g., Yu, 1984; Qi and Shi, 1999; Li et al., 2012). As for the spatial distributions of the SWH in the four seasons, there is also a debate. During the winter northeasterly monsoon, most researchers agree that the SWH is the largest in the northern SCS, and basically decreases southward across the ocean basin (e.g., Yu, 1984; Chen, 1987; Qi et al., 1997; Chen et al., 2006; Li et al., 2012; Wu et al., 2014; and others), while some numerical results support that it is the largest in the central/southern SCS (e.g., Zhou et al., 2007; Zong and Wu, 2014). During the summer southwesterly monsoon, the debate is similar. On one hand, some researches indicate that the SWH is larger in the central/southern SCS than in the northern SCS (e.g., Yu, 1984; Qi et al., 1997; Zhou et al., 2007; Zong and Wu, 2014). On the other hand, a lot of studies demonstrate that the SWH in this season is the largest in the northern SCS (e.g., Gulev et al., 2003; Chen et al., 2006; Li et al., 2012; Wu et al., 2014).

Foundation item: The Shandong Provincial Natural Science Foundation under contract Nos ZR2015DQ006 and ZR2014DQ005; the National Natural Science Foundation of China under contract Nos 41506008 and 41476002; the China Postdoctoral Science Foundation under contract No. 2015M570609.
*Corresponding author, E-mail: gfzhai@ouc.edu.cn

Therefore, the major goal of the current study is to investigate the seasonal variation of the SWH in the SCS using the most up-to-date gridded observations merged from all available satellite missions. Then we attempt to examine the contributions of swell and wind sea to the seasonal SWH variations using the method proposed by Chen et al. (2002). At last, the seasonal variation of extreme wave conditions is discussed. The outline of this paper is as follows: Data and methods are described in Section 2; Section 3 gives the results; and Section 4 presents the summary and discussion.

2 Data and methods

2.1 *Satellite altimeter data and wind reanalysis*

The satellite altimeter data used in the current study are the near-real-time gridded SWH with a horizontal resolution of 1.0°×1.0° from the multimission merged product of Aviso (http://www.aviso.altimetry.fr/en/home.html). The altimeter missions that are used to prepare the data product include GEOSAT, ERS-1, ERS-2, TOPEX, Jason-1, Jason-2, ENVISAT, and so on. A merged map of the SWH is generated only when there are at least two missions available and the data are cross-calibrated using OSTM/Jason-2 as reference mission (http://www.aviso.altimetry.fr/en/home.html). The merged SWH lasts from September 14, 2009 to present with a time interval of one day, and the data before September 2015 are used here to examine the seasonal wave height variability in the SCS.

Along with the SWH data, Aviso has also provided merged gridded observations of the sea surface wind speed. However, as stated in Chen et al. (2002), the altimeter wind speed measurements can be considerably affected by long waves. Therefore to help the current analysis, we adopt the wind speeds at 10 m above the sea surface from the ERA Interim (ERA-I) (Dee et al., 2011) reanalysis, which is the most up-to-date global atmospheric reanalysis produced by the European Center for Medium-Range Weather Forecasts (ECMWF). The ERA-I sea surface winds are downloaded from http://apps.ecmwf.int/datasets/data/interim-full-daily/levtype=sfc/ with a time interval of 6 h and a horizontal resolution of 0.125°×0.125°. For easy comparison, the 6 h sea surface winds are averaged to get the daily means for the same period to the merged SWH.

Figure 1 shows the climatological SWH and surface wind speeds. As shown in Fig. 1a, there is a tongue of high SWH that extends from the western North Pacific Ocean into the SCS through the Luzon Strait (LS). Therefore the SWH in the SCS is highest around the LS and then gradually decreases southwestward across the basin, consistent with previous observations (e.g., Yu, 1984; Gulev et al., 2003; Chen et al., 2006), numerical simulations (e.g., Zheng and Zhou, 2012; Zheng and Li, 2015), and also global wave reanalysis (e.g., Wu et al., 2014). The mean SWH in the northern SCS is generally above 1.5 m, while that in the southern shelf region is lower than 1.0 m. The climatological mean surface wind speed shows similar spatial distributions, generally strong in the northern and central SCS while weak in the southern SCS (Fig. 1b). Instead of monotonically decreasing southwestward across the SCS Basin, however, the surface wind speed shows local maxima in two regions, one locating around south of Taiwan Island and the other southeast of Vietnam Coast (around 9°–12°N, 108°–111°E). The maximum wind speeds in the two regions are both about 7.7 m/s.

In Fig. 1c, we compare the monthly time series of the area-averaged SWH and the surface wind speed over the whole SCS

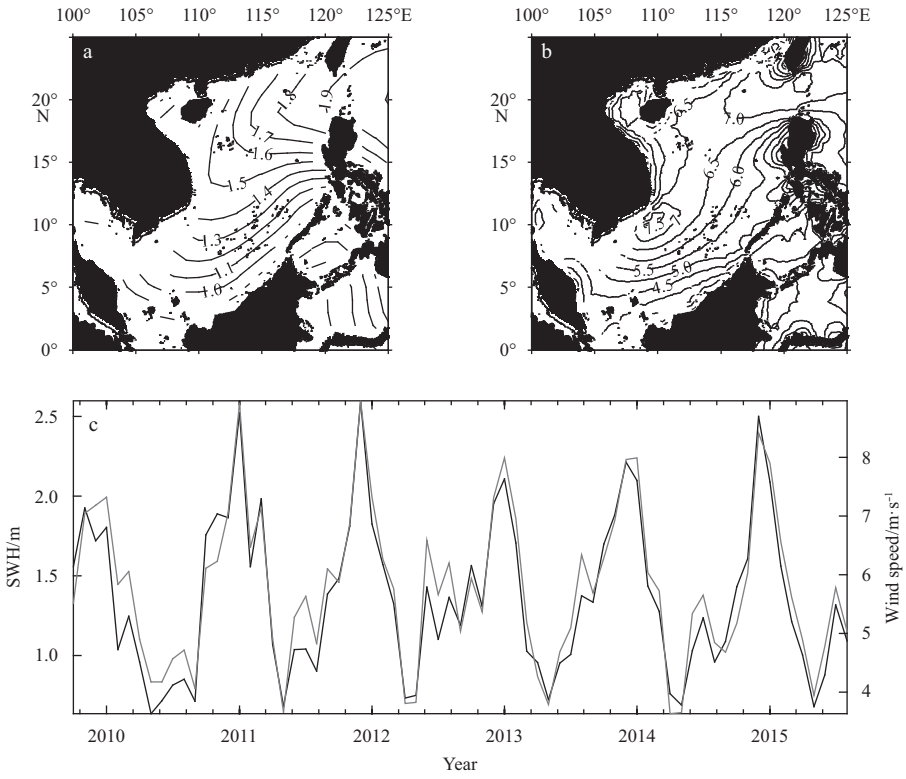

Fig. 1. Comparison of the SWH and sea surface wind speed in the SCS. a. Climatological SWH (m). The contour interval is 0.1 m. b. Climatological ERA-I wind speed at 10 m above the sea surface (m/s). The contour interval is 0.5 m/s. c. Monthly time series of the SWH (black line) and surface wind speed (gray line) averaged over the whole SCS from October 2009 to August 2015.

Basin. As we can see, the two time series agree quite well with each other. Their linear correlation coefficient is about 0.96 above the 95% confidence level, indicating significant in-phase variations both on the seasonal and interannual time scales. Another prominent feature in this figure is that the SWH shows similar significant seasonal variations in all the six years of interest, generally being the largest in winter and the smallest in boreal spring. And the most important is that the seasonal variation obviously dominates the monthly time series (e.g., Chen et al., 2006).

Figure 2 shows the standard deviation (STD) of the monthly SWH and surface wind speed calculated over the whole period. Interestingly, the two variables show quite similar spatial variations, both have a band of high values along a northeast-southwest tilt line from the southwest of Taiwan Island to southeast of Vietnam Coast. There are two local maxima locating in the northeastern and southwestern parts of the band, respectively, for both SWH and wind speeds. Carefully inspecting the figures, one can see that the northern/southern local maximum of the SWH is slightly south/north of that of the surface wind speed. The largest STD of the monthly mean SWH is about 0.64 m and appears around 17.5°N, 116°E. The STD maximum of the monthly SWH just east of the Vietnam Coast is about 0.61 m and located around 12°N, 110.5°E. On the other hand, the largest STD of the monthly mean surface wind speed is about 2.2 m/s and occurs around 19°N, 118°E. The STD maximum of the monthly surface wind speed southeast of the Vietnam Coast is about 2.1 m/s and located around 10.2°N, 109.7°E.

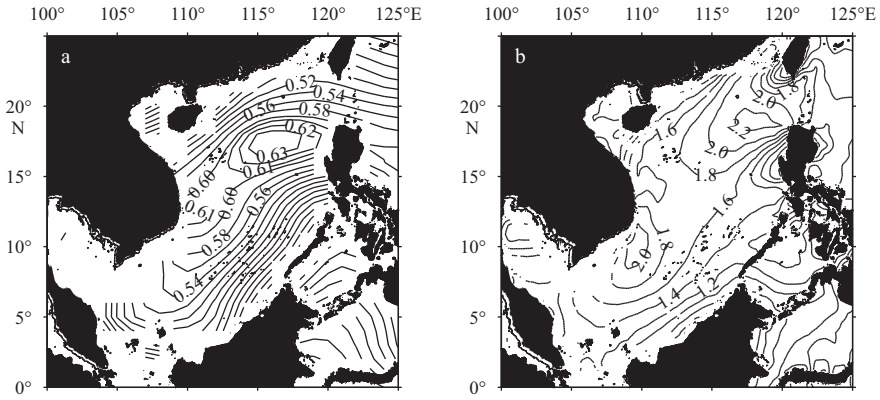

Fig. 2. Standard deviations of the monthly mean SWH (m) (a) and surface wind speed (m/s) (b). In Fig. 2a, the contour interval is 0.02 m for the SWH smaller than 0.60 m and 0.01 m for the SWH larger than 0.61 m. In Fig. 2b, the contour interval is 0.2 m/s.

2.2 *Methods*

The satellite observed SWH is the sum of contributions from wind sea and swell. In the present study, the SWHs of the wind sea and swell are separated using the method proposed by Chen et al. (2002). The SWH and the sea surface wind speed, based on previous studies, follow a monotonical relationship under a growing sea up to the fully developed stage. Many methods have been developed to calculate the SWH for fully developed seas (e.g., Sverdrup and Munk, 1947; Pierson and Moskowitz, 1964; Ewing and Laing, 1987; Hasselmann et al., 1988; Pierson, 1991). Among them, the WAM-derived expression has an intermediate overall growth rate for the wind speed ranging from 0 to 50 m/s (Pierson, 1991), and is thus deemed to be the most appropriate (Chen et al., 2002). The SWH ($H_{\mathrm{sw,\,w}}$) for fully developed seas, according to the WAM results (Hasselmann et al., 1988), is expressed as

$$H_{\mathrm{sw,\,w}} = 1.614 \times 10^{-2} U^2 \quad \text{for } 0 \leqslant U < 7.5 \text{ m/s}, \tag{1a}$$

$$H_{\mathrm{sw,\,w}} = 10^{-2} U^2 + 8.134 \times 10^{-4} U^3 \quad \text{for } 7.5 \text{ m/s} \leqslant U < 50 \text{ m/s}, \tag{1b}$$

where U is the ERA-I wind speed at 10 m above the sea surface.

The observed SWH which is smaller than the $H_{\mathrm{sw,\,w}}$ is seen from a growing sea, while that larger than the $H_{\mathrm{sw,\,w}}$ is quite probably swell dominated (Chen et al., 2002). Though being not necessarily to be valid in an absolute sense due to the complexity of the wind-swell coupling, the above inference is expected to give a meaningful classification of the two regimes from a statistical point of view (Chen et al., 2002). Then two probability indices can be defined to quantify the frequencies of occurrences of the wind sea and swell as

$$P_{\mathrm{s}} = N_{\mathrm{s}}/N, \tag{2a}$$

$$P_{\mathrm{w}} = N_{\mathrm{w}}/N, \tag{2b}$$

where N_{s} and N_{w} are the numbers of swell and wind sea dominated events; and N is the total number of data points. As N=N_{s}+N_{w}, P_{s}+P_{w}=1. Statistically describing the proportions of dominance of the swell and wind sea, the swell and wind sea probabilities can also be statistically approximated to the energy proportions of the swell and wind sea to the total sea surface wave energy (e.g., Chen et al., 2002; Jiang and Chen, 2013). Based on the above assumption and considering that the wave energy is proportional to the square of SWH, the swell height (H_{s}) and wind sea height (H_{w}) can be estimated from the SWH (H_{sw}) as follows:

$$H_{\mathrm{s}} = H_{\mathrm{sw}} \sqrt{P_{\mathrm{s}}} \ , \tag{3a}$$

$$H_{\mathrm{w}} = H_{\mathrm{sw}} \sqrt{P_{\mathrm{w}}} \ . \tag{3b}$$

The above method has been used in many studies (e.g., Chen et al., 2002; Zhang et al., 2011; Jiang and Chen, 2013; Anoop et al., 2015; Shanas and Kumar, 2015).

In this paper, the seasons always refer to those for the Northern Hemisphere; for example, summer refers to June, July and August, and winter refers to December, January and February.

3 Results

3.1 *SWH and wind speed*

As the first expression, we give in Fig. 3a the climatological monthly SWH averaged over the whole SCS. From the figure, we can see that the SWH is the largest in December, while the smallest in May. This is consistent with previous observations (e.g., Yu, 1984; Qi and Shi, 1999) and numerical simulations (e.g., Zhou et al., 2007; Li et al., 2012). The SWH decreases rapidly from January to May, then increases slowly from June to September, and at last increases rapidly from September to December. Figure 3b shows the STD of the climatological monthly SWH in the SCS, denoting the strength of the seasonal variability. As expected, the STD of the climatological monthly mean SWH, though being slightly smaller, exhibits nearly the same spatial distribution to that of the monthly SWH as shown in Fig. 2a. The two high STD regions are same to those for the monthly time series (Fig. 2a). The largest STDs in the two regions west of the Luzon Island and east of Vietnam Coast are about 0.58 and 0.56 m, respectively, both slightly smaller than those for the monthly time series. This further confirms that the seasonal variation dominates the SWH variations in the six years of interest (e.g., Chen et al., 2006).

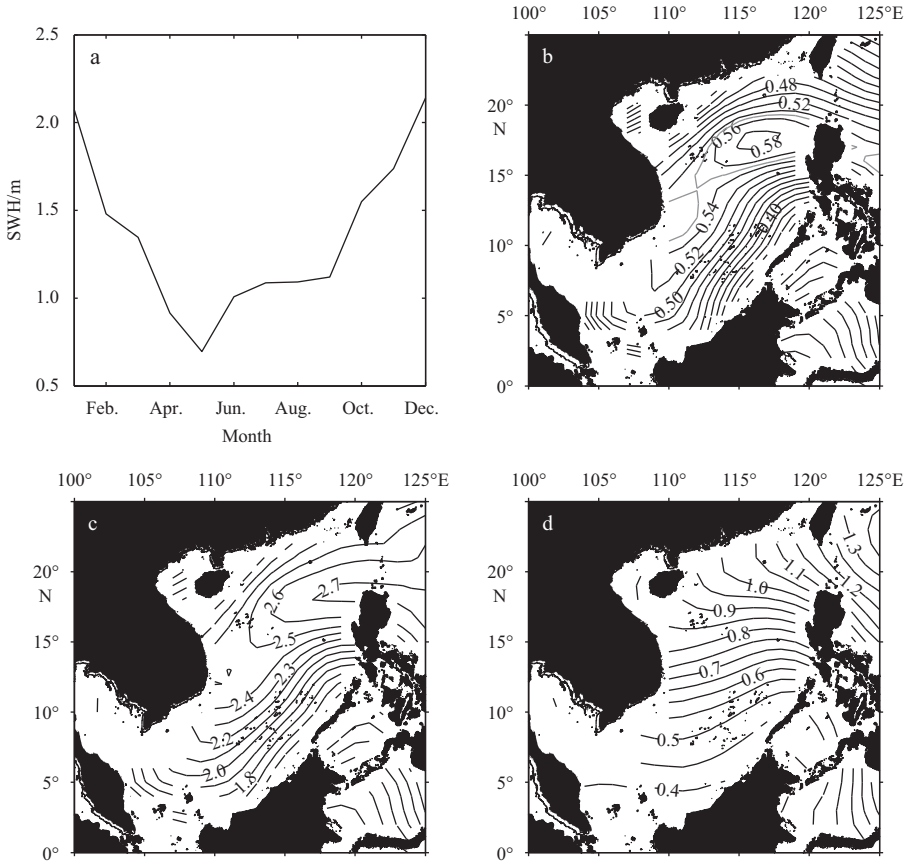

Fig. 3. Seasonal climatology of the SWH. a. The climatological monthly time series of the SWH averaged over the whole SCS; b. the STD of the climatological monthly SWH in the SCS. The interval for black contours is 0.02 m. The gray line denotes the 0.55 m contour. c. The maxima of the climatological monthly SWH. The contour interval is 0.10 m. d. The minima of the climatological monthly SWH. The contour interval is 0.05 m.

Figures 3c and d exhibit the climatological annual maxima and minima of the SWH in the SCS, respectively. Generally, both of them share similar spatial variations to the climatological mean SWH as shown in Fig. 1a, decreasing southward across the SCS Basin from the LS. However, there is also difference. The spatial variation of the climatological annual maximum SWH is more like that of the climatological mean SWH, with the high SWH tongue extending from the LS to the southern SCS. The climatological annual minimum SWH, however, has its isolines tilting from southeast to northwest in the northern SCS while from northeast to southwest in the southern SCS. In the SCS, the annual maximum SWH basically ranges from 1.7 to 2.7 m, while the annual minimum SWH ranges from 0.4 to 1.2 m.

Another interesting thing is that the whole SCS exhibits a uniform seasonal variation in the SWH, with the maxima occurring in December/January and minima in May, consistent with that shown in Fig. 3a and previous studies (e.g., Yu, 1984; Qi and Shi, 1999; Li et al., 2012). On the other hand, however, there are many studies stating that the SWH is weakest in summer when considering the climatological seasonal means (e.g., Qi et al., 1997; Chen et al., 2006; Zhou et al., 2007). This is different from our current study. Actually, when considering the climatological seasonal means, the observed SWH is the largest in winter ranging from 1.5 to 2.4 m. In autumn, the SWH ranges from 0.9 to 2.2 m, slightly smaller than that in winter. And the SWH is weakest in spring and summer. In the two seasons (Figs 4a and b), the observed SWH ranges from 0.7 to 1.5 m, much smaller than those in winter and autumn. Figure 4c presents the difference of the SWH between summer and spring. From the figure, we know that the SWH in summer is generally larger than that in spring in regions

south of about 16°N, while in regions north of 16°N the situation is reversed. The largest positive difference is about 0.5 m occurring around 12°N, 115.5°E in the central SCS. Therefore, the climatological SWH is weakest in summer in the northern SCS north of about 16°N, while in spring in other regions. Figure 4d compares the climatological monthly SWHs averaged over regions north (black line) and south (gray line) of 16°N. In the northern SCS, the mean SWH in spring is larger than that in summer by about 0.04 m, while in the central/southern SCS the former is smaller than the latter by about 0.14 m.

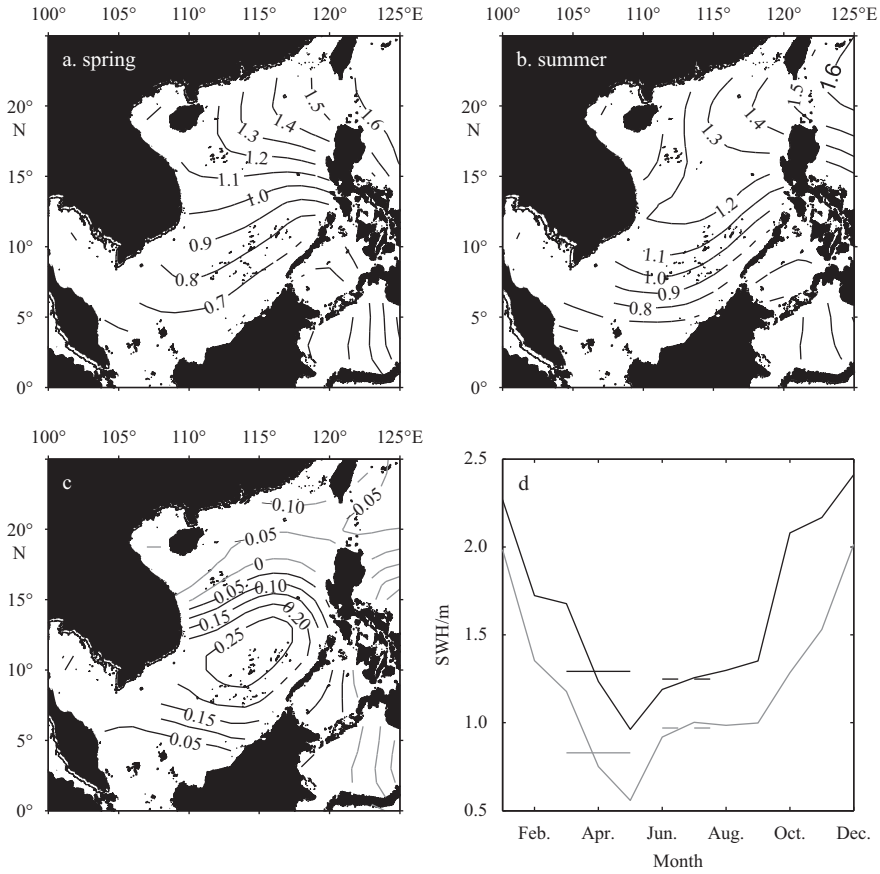

Fig. 4. Climatological seasonal mean SWH (m) in spring (a) and summer (b) (contour interval: 0.1 m) and the difference of SWH between summer and spring (c) (contour interval: 0.05 m). Climatologcial monthly mean SWH averaged over regions north of 16°N (black line) and south of 16°N (gray line) (d). Thick solid and dashed lines denote the seasonal mean SWHs averaged in spring and summer seasons, respectively.

Besides, in all the four seasons, the observed SWH in the SCS is the largest around the LS and then gradually decreases southward across the basin. This is consistent with previous results derived from satellite and ship observations (e.g., Chen et al., 2006; Gulev et al., 2003), model hindcasts (e.g., Li et al., 2012), and wave reanalyses (e.g., Wu et al., 2014). However, it is quite different from the picture derived by some other studies (Yu, 1984; Qi et al., 1997; Zhou et al., 2007). Using ship observations, Yu (1984) reported that the SWH decreases from north to south during the northeasterly monsoon, while is the largest in the central SCS during the southwesterly monsoon. Analyzing outputs of the numerical simulation conducted with the WAVEWATCH-III model (Tolman, 1990), Zhou et al. (2007) pointed that the largest SWH occurs in the ocean interior far away from the LS in all the four seasons. With the observations obtained by GEOSAT, Qi et al. (1997) indicated that the SWH in summer is larger in the southern SCS than in the northern SCS and there is a region around 10°N, 110°E with high SWH throughout the year, which is absent in our current study. The differences between our current study and previous observations are possibly because the latter are obtained either by individual ships or by only one satellite mission and thus may contain considerable errors (e.g., Gulev et al., 2003; Semedo et al., 2011). On the other hand, the difference between the present study and that derived by Zhou et al. (2007) is possibly due to errors in model outputs, which are not constrained by observations and also the small model domain they adopted (see Section 4).

With the significant seasonality in the SWH, it is also useful to examine the seasonality in the sea surface wind speed. Figure 5a displays the climatological monthly wind speed averaged over the whole SCS Basin. Overall, the sea surface wind speed shows the same seasonality to the SWH, being the strongest in December/January and the weakest in May. However, it also has a weak maximum in July and a weak minimum in September. The maxima in winter and summer correspond to the peak phases of the northeasterly and southwesterly monsoons, respectively; while the minima in May and September are associated with the two sharp transitions (e.g., Yu, 1984; Tao and Chen, 1987; Qi and Shi, 1999; Fang et al., 2002; Ha et al., 2012; Zhai et al., 2014).

Figure 5b shows the STD of the climatological monthly mean sea surface wind speed in the SCS, presenting the strength of the seasonal variability. As expected, the STD of the climatological

monthly sea surface wind speed is also nearly the same to that of the monthly counterpart as shown in Fig. 2b. Figures 5c and d give the annual climatological maxima and minima of the surface wind speed in the SCS, respectively. Generally, the annual maximum wind speed shares similar spatial variations to the climatological mean wind speed as shown in Fig. 1b. There are two regions with high wind speed locating southwest of Taiwan Island (around 19.5°N, 117.4°E) and southeast of Vietnam Coast (around 10.5°N, 109.7°E), respectively. The largest wind speeds in these two regions are 10.6 and 11.1 m/s, respectively. On the other hand, the annual minimum wind speed is the largest in the northwestern SCS and then decreases both eastward and southward.

The annual maximum wind speed occurs in December/January for the whole SCS basin (figure not shown). The annual minimum wind speed appears in May for most regions of the SCS, while in April and September in two small regions east of Vietnam around 15°N, which is different from the minimum SWH. Considering the four seasons in the year, the climatological seasonal mean wind speed is the largest in winter ranging from 5.0 to 10.0 m/s. In autumn it ranges from 4.0 to 8.0 m/s and is slightly smaller than that in winter. The seasonal mean wind speeds in both winter and autumn (figure not shown) share similar spatial distributions to the climatological annual maximum wind speed (Fig. 5c). Both have high values in regions southwest of Taiwan Island and southeast of the Vietnam Coast. The maximum wind speeds in the two regions are 9.4 and 10.0 m/s in winter, while 8.5 and 7.2 m/s in autumn, respectively.

As shown in Fig. 5a, the SCS averaged sea surface wind speeds in spring and summer are much smaller than those in winter and autumn. We then compare the mean surface wind speeds in the two seasons in Fig. 6. In spring, the surface wind speed basically decreases from north to south (Fig. 6a). Southeast of the Vietnam Coast there is still a small region with higher wind speed than surrounding areas. However, the maximum wind speed in that region is only about 5.9 m/s, much smaller than those in other three seasons. On the contrary, the surface wind speed in summer (Fig. 6b) is the the largest in the central SCS and decreases both northward and southward (e.g., Xie et al., 2003; Chu et al., 2004). Figure 6c gives the difference of the surface wind speed between summer and spring, which exhibits a meridional dipole structure. Therefore, the surface wind speed is larger in summer than in spring in the central/southern SCS, while the situation is reversed in the northern SCS. Indeed, in the northern SCS the mean surface wind speed in spring is larger than that in summer by about 0.06 m/s, while in the central/southern SCS the former is smaller than the latter by about 0.91 m/s.

At last, we should note that the surface wind speed is also larger in summer than in autumn in most regions south of about 14°N (figure not shown), due to the strong southwesterly monsoon (e.g., Tao and Chen, 1987). Therefore, the surface wind speed is weakest in summer in the northern SCS, while in spring in the central/southern SCS. This, to a large extent, explains why

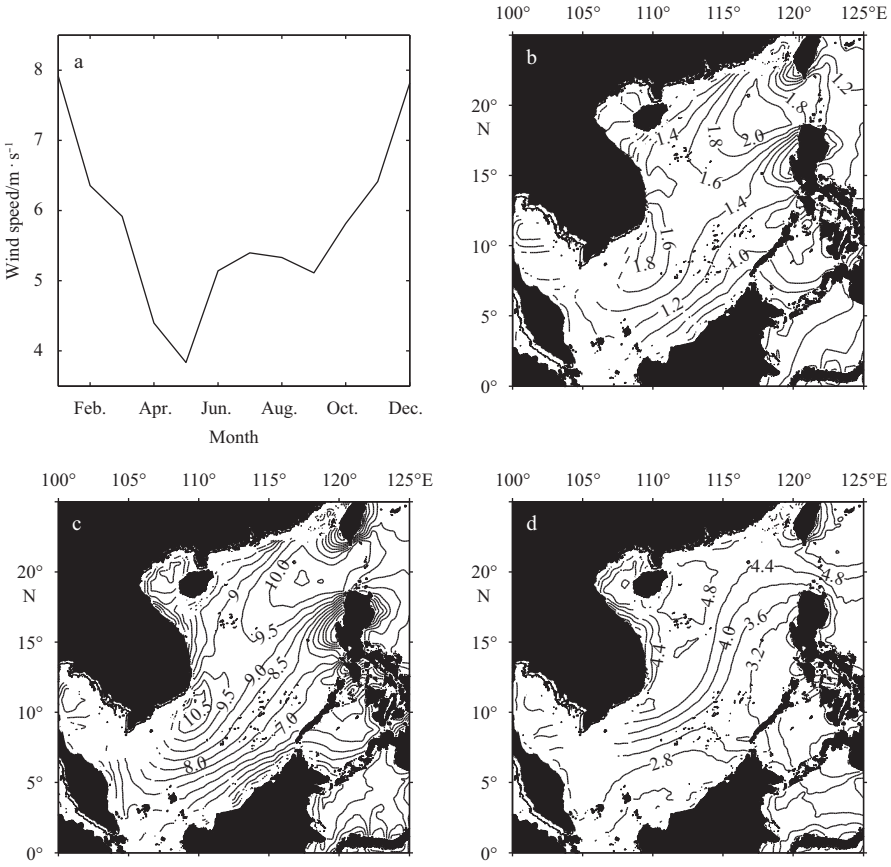

Fig. 5. Seasonal climatology of the ERA-I sea surface wind speed. a. The climatological monthly time series of the sea surface wind speed averaged over the whole SCS; b. the STD of the climatological monthly sea surface wind speed in the SCS, the contour interval is 0.20 m/s; c. the maxima of the climatological monthly sea surface wind speed, the contour interval is 0.50 m/s; d. the minima of the climatological monthly sea surface wind speed, the contour interval is 0.40 m/s.

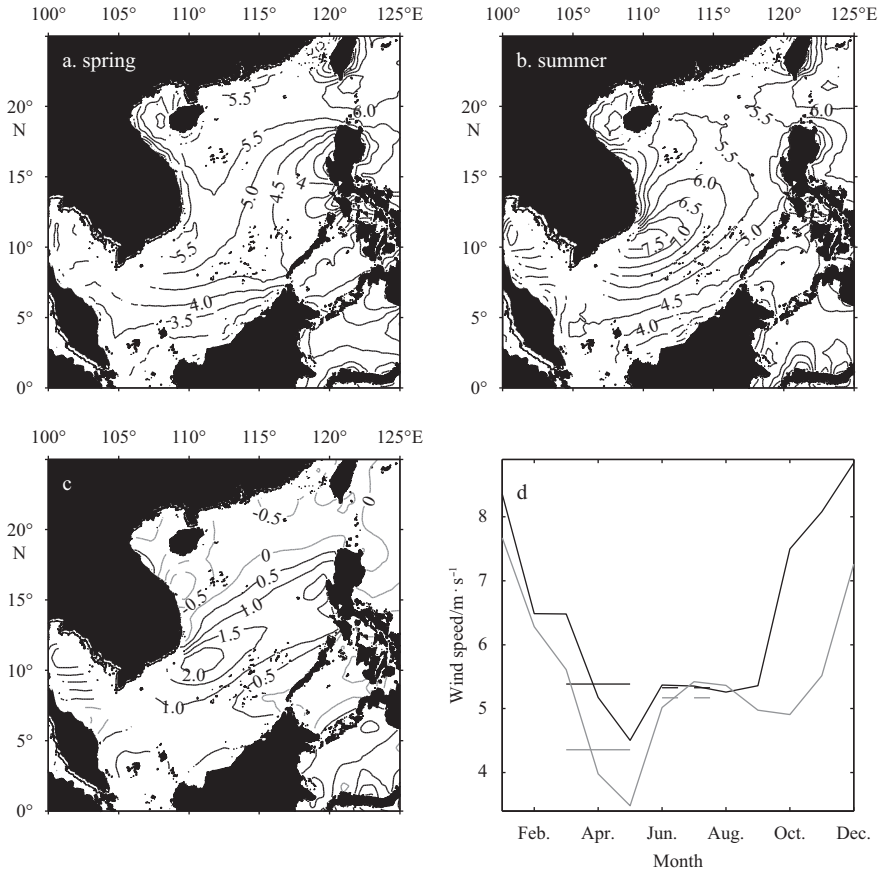

Fig. 6. Climatological seasonal mean ERA-I wind speed (m/s) at 10 m above the sea surface in spring (a) and summer (b) (contour interval: 0.50 m/s) and the difference of the sea surface wind speed between summer and spring (c) (contour interval: 0.50 m/s). Climatologcial monthly mean sea surface wind speed averaged over regions north of 16°N (black line) and south of 16°N (gray line) (d). Thick solid and dashed lines denote the seasonal mean surface wind speeds averaged in spring and summer seasons, respectively. In Fig. 6d, the summer mean wind speed to the south of 16°N (thick dashed gray line) is subtracted 0.1 m/s for clarity.

the SWH is weakest in summer in the northern SCS, while in spring in the central/southern SCS (Fig. 4).

3.2 *Swell and wind sea height analyses*

According to Eq. (1), for the fully developed seas, the SWH would be controlled solely by local sea surface winds, which means that the seasonal variation of the SWH would completely follow that of the sea surface wind speed. Overall, as shown in the above subsection, the temporal variation of the SWH on the seasonal time scale shows quite good correspondence with that of the surface wind speed. However, there are also significant differences between the seasonal variations of the two variables, especially in their spatial distributions. The biggest difference is that, in summer the SWH is the largest around the LS and then decreases from north to south (Fig. 4b), while the surface wind speed is the largest in the central SCS (Fig. 6b). On the other hand, the spatial distributions of the annual maxima and STD of the SWH (Fig. 3) are also different from those of the surface wind speed (Fig. 5). Besides, the disagreement of the SWH with the sea surface wind speed in the SCS has also been noted by Chu et al. (2004) and Li et al. (2012). All of these imply that the observed SWH is not always dominated by the wind sea throughout the year. Indeed, using satellite observations, Chen et al. (2002) indicated that the global ocean was mostly dominated by the swell. And according to their climatology, the swell probability in the SCS is well above 80%. In another study (Hanley et al., 2010), which uses the inverse wave age to determine the ocean being either in the wind-driven wave regime (wind sea) or in the wave-driven wind regime (swell), the authors also argued that the swell is more prevalent in the tropics. From their climatology of the inverse wave age, the sea state in the SCS is always composed by both wind sea and swell. Therefore, it is useful for the current study to examine the probabilities of the swell and wind sea and calculate their wave heights using the merged satellite observations.

Figure 7a displays the swell probability during the whole period of observations. In the SCS the swell probability is well above 67%, proving the swell dominance. Its spatial variation is well opposite to that of the sea surface wind speed, showing small probabilities in regions with high sea surface wind speeds (Fig. 1b). Figure 7b gives the STD of climatological monthly swell probabilities. For each month, the climatological swell probability is calculated using pairs of SWH and sea surface wind speed of that month throughout 6 a. As shown in the figure, the STD is well below 0.05 for most regions in the SCS, implying small seasonal variations. Besides, we also note two regions with high STD values around (9°–12°N, 110°–113°E) and (17°–20°N, 116°–119°E), respectively. As shown in Fig. 5b, these two regions also show high STD values of the climatological monthly sea surface wind speed. This may indicate the large wind sea contribution in the seasonal

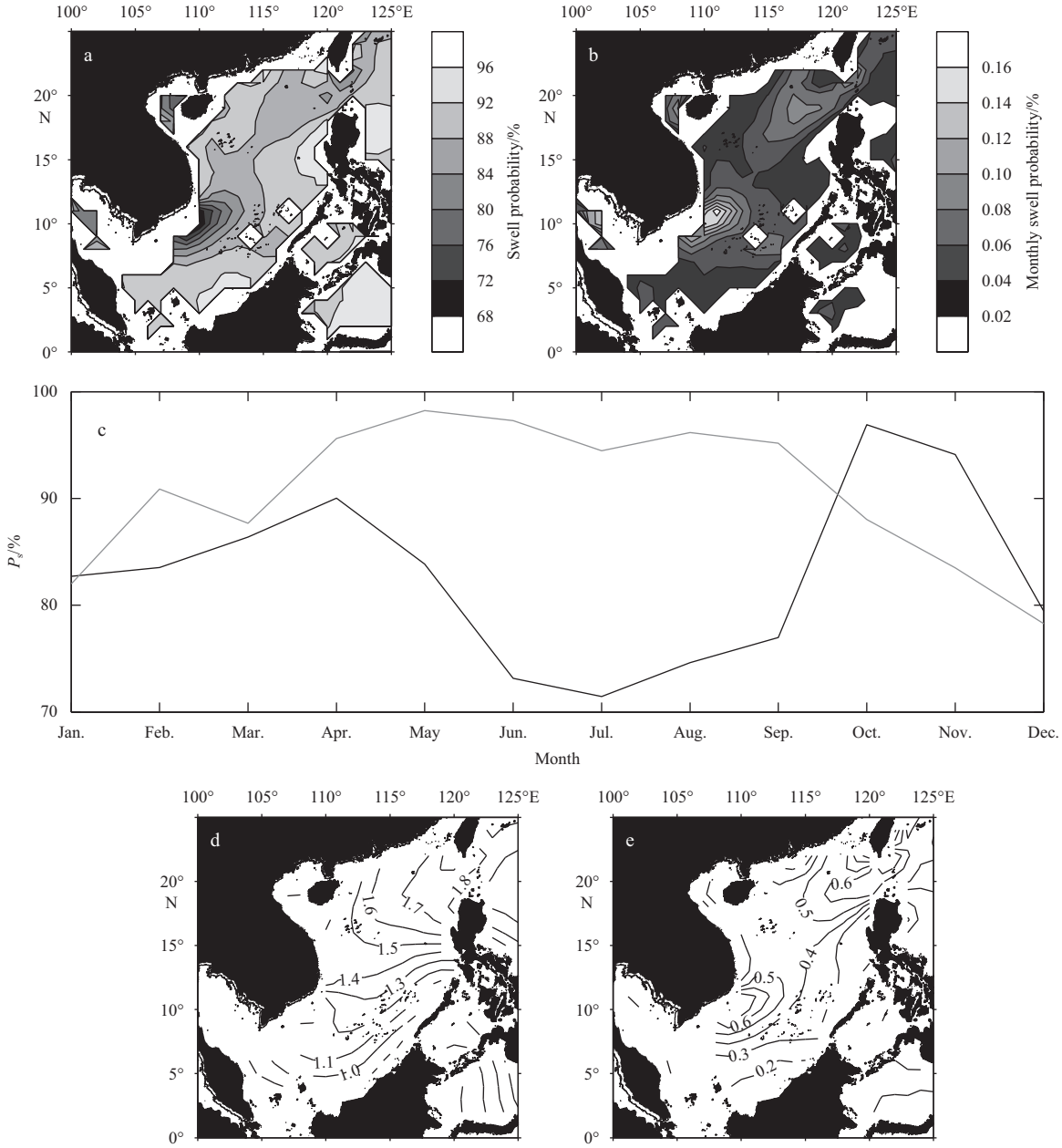

Fig. 7. The swell probability (%) calculated over the whole period (a); the STD of climatological monthly swell probability(%) (b); the climatological monthly swell probabilities (%) averaged over two regions 9°–12°N, 110°–113°E (black line) and 17°–20°N, 116°–119°E (gray line) (c); the climatological swell height (m) (d); and the climatological wind sea height (m) (e).

variations there. The climatological monthly time series of the swell probability averaged over the two regions are shown in Fig. 7c. Basically, the swell probability averaged in the region southwest of Taiwan Island is the largest in boreal spring and the smallest in winter, while that averaged in the region southeast of Vietnam has two maxima in April and October and two minima in July and December, respectively. These are well associated with the strong seasonal variations of the sea surface wind speeds in the two regions (Fig. 5a).

With the climatological monthly probabilities of the swell and the wind sea, we calculate the wave heights of the swell and the wind sea according to Eq. (3). As one can expected, in the SCS the swell wave height (Fig. 7d) ranges from 1.0 to 1.8 m and is generally much larger than the wind sea height (Fig. 7e), which ranges from 0.2 to about 0.8 m. That in the SCS the swell height is larger than the wind sea height is consistent with previous ship observations (Yu, 1984; Gulev et al., 2003) and the global climatology (e.g., Semedo et al., 2011) derived from the 45 a ECMWF reanalysis (ERA-40) (Uppala et al., 2005). Though being slightly smaller, the swell height basically has the same spatial distribution to that of the climatological mean wave height (Fig. 1a). On the other hand, the spatial distribution of the wind sea height is highly like that of the sea surface wind speed (Fig. 1b), with two regions of large wind sea height locating southwest of Taiwan Island and southeast of Vietnam Coast, respectively.

Figure 8 compares the seasonal variations of the swell and wind sea wave heights. As shown in the figure, the seasonal wave height variations of both the swell and the wind sea are like those of the merged SWH (Fig. 3). They are the largest in winter for the whole SCS, while weakest in summer in the northern SCS and in

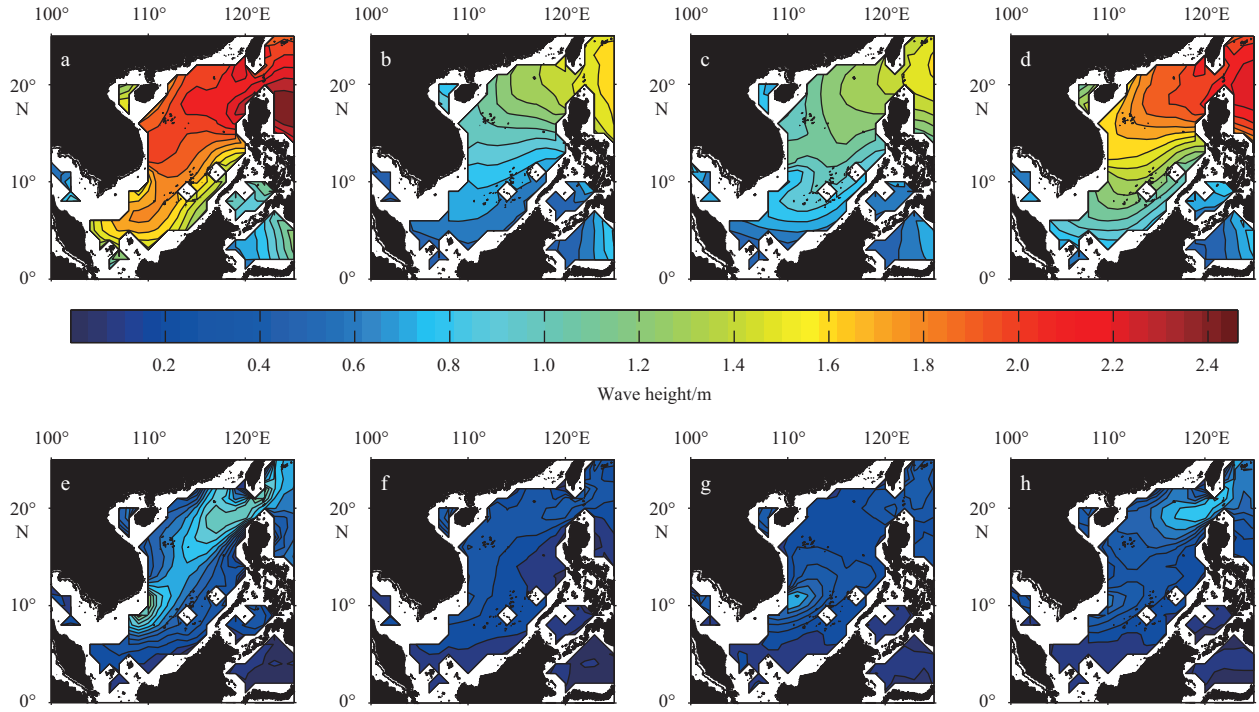

Fig. 8. Wave heights of the swell (a–d) and wind sea (e–h) in the four seasons: winter (a and e), spring (b and f), summer (c and g), and autumn (d and h). The contour interval is 0.1 m.

spring in the central/southern SCS. The spatial distributions of the swell height in the four seasons are consistent with those of the merged SWH. The wind sea height, on the contrary, shows different spatial variations. In fact, its spatial variation is quite like that of the surface wind speed. During the northeasterly monsoon, the wind sea height is the largest in two regions southwest of Taiwan Island and southeast of Vietnam Coast, while during the southwesterly monsoon it has higher values in the central/southern SCS (e.g., Semedo et al., 2011).

Using observations obtained by individual ships, Yu (1984) pointed out that the swell height ranged from about 1.0 m in the southern SCS to above 2.0 m in the central/northern SCS during winter monsoon, while from 1.0 to about 2.0 m in most regions in the SCS during summer monsoon. His results agree well with the swell height derived from merged satellite observations in terms of both the temporal variation and exact values (Figs 8a and c). On the other hand, he also indicated that the wind sea height ranged from 1.0 to 2.0 m in the northern SCS, 1.0 to 1.5 m in the central SCS, and was about 1.0 m in the southern SCS during the winter monsoon, while is about 1.0 m in the northern SCS, about 1.2 m in the central SCS, and about 0.8–1.2 m in the southern SCS during the summer monsoon. As shown in Figs 8e and g, the wind sea heights obtained in the current study are much smaller than those obtained by Yu (1984) in both monsoon seasons and the climatology obtained by Gulev et al. (2003). This is possibly due to errors contained in ship observations (e.g., Gulev et al., 2003) and also because that for each grid point much more samples have been used in preparing the merged satellite observations, which could possibly results in smaller averages.

3.3 *Extreme wave conditions*

Another important question related to the wave climate in the SCS that has been rarely studied before is about the variations of extreme wave conditions, which are crucial for the design of coastal and offshore infrastructures, navigation, coastal management, and so on (e.g., Sasaki et al., 2005; Izaguirre et al., 2011). In the current study, the seasonal variability of the SWH at the 99th percentile is studied. Figures 9a and b give the 99th percentiles of the SWH and the sea surface wind speed for the whole period of interest, respectively. In the SCS, the 99th percentile of the SWH shows significant spatial variations, being large (>4.4 m) along a band extending from northwest of Luzon Island to northeast of Vietnam Coast, and then decreasing both northward and southward. Its maximum value is about 4.9 m and appears around (17.5°–18.5°N, 115°–118°E). The spatial distribution of the 99th percentile of SWH derived here is roughly consistent with those from ERA-40 global reanalysis and a coupled atmosphere-wave model hindcast (Fan et al., 2012).

In the northern SCS, the 99th percentile of the sea surface wind speed shows similar distribution to the 99th percentile of the SWH, with a high value band extending from northwest of Luzon Island to northeast of Vietnam coast (Fig. 9b). The maximum sea surface wind speed of 16.5 m/s occurs around (17.5°–19.5°N, 117.5°–120.5°E), slightly east of the maximum SWH. Then the surface wind speed generally decreases both northward and southward. In a small area southeast of Vietnam Coast, however, it exhibits higher values than surrounding areas. Further analysis indicates that the extreme high SWH and sea surface wind speed mainly appear in the autumn (September, October, and November).

We then calculated the $H_{sw,\,w}$ using the 99th percentile of the surface wind speed and compare it with the 99th percentile of the observed SWH. Shown as gray points in Fig. 9a, the $H_{sw,\,w}$ larger than the observed SWH is mainly located in the northern SCS west of the LS and in a small area southeast of Vietnam Coast, where the 99th percentile of the surface wind speed is also relatively large (Fig. 9b).

Figure 10 gives the seasonal variation of the 99th percentile of

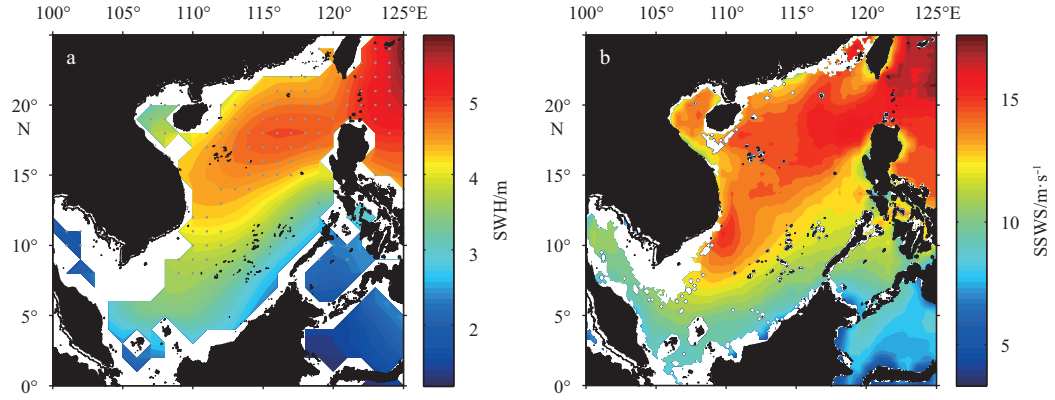

Fig. 9. The 99th percentiles of the SWH (a) and sea surface wind speed (SSWS) (b). In Fig. 9a, regions with $H_{sw,\,w}$ larger than the observed SWH are shown as gray points.

the SWH. Calculated with all grid points in the SCS, the 99th percentile of the SWH has its maximum in October and minimum in May (red line in Fig. 10a). We then calculate the $H_{sw,\,w}$ with the climatological monthly surface wind speed at the 99th percentile, which is shown as the blue line in Fig. 10a. Overall, the $H_{sw,\,w}$ is larger than the observed SWH in September-December. This indicates that the observed 99th percentile of the SWH is dominated by the wind sea in these months, while by the swell in other months. A large region centering around (16°N, 112°E) in the northern SCS has the largest seasonal variation in the 99th percentile of the SWH (Fig. 10b). The largest STD of the climatological monthly SWH at the 99th percentile in that region can be as high as 1.3 m. In the southern SCS, the 99th percentile of the SWH is relatively low. However, it also shows high values (>0.9 m) in a small region around (5°–7°N, 106.5°–109°E). The spatial distribution of the 99th percentile of the SWH is different from that of the sea surface wind speed (figure not shown). The largest seasonal variation in the surface wind speed at the 99th percentile occurs just west of the LS, about 4°–6° east of that in the SWH at the same percentile. This further confirms that the 99th percentile of the SWH is dominated by the wind sea or swell in different seasons.

Figures 10c and d give the maxima and minima of the climatological monthly SWH at the 99th percentile in the SCS, respectively. Generally, both of them decreases southward. The SWH climatological monthly maxima range from 3.0–4.0 m in the southern SCS to well above 5.0 m in the northern SCS. The largest value is about 5.9 m and occurs around (18°N, 116°E) in the northern SCS. The SWH climatological monthly minima in the SCS, on the other hand, are well below 2.5 m and even below 2.0 m for most regions. As shown in Figs 10e and f, the maxima of the climatological monthly 99th percentile SWH mainly appear in August–November in most regions of the northern and central SCS and in December/January in the southern SCS, while the minima mainly appear in May. Therefore, the 99th percentile SWH shows similar seasonal variation to the climatological monthly mean SWH except in the northern/central SCS.

We then calculate the $H_{sw,\,w}$ with the maxima of the climatological monthly sea surface wind speed at the 99th percentile, and then compare it with those of the SWH at the same percentile. As indicated by the gray dots in Fig. 10c, the calculated $H_{sw,\,w}$ in the northern/central SCS is well larger than the observed 99th percentile of the SWH. This proves that the SWH climatological monthly maxima at the 99th percentile are dominated by wind seas.

As the mean surface wind speed is smaller in autumn than in winter, that the maxima of the 99th percentile of the SWH in the northern/central SCS occur in boreal summer and autumn is obviously associated with tropical cyclone (TC) activities. Indeed, in the SCS and the western North Pacific Ocean the active TC season is from July to November (e.g., Li, 1988; Chia and Ropelewski, 2002; Liu and Chan, 2003; Chan, 2005; Wang et al., 2007). Moreover, most of TCs in the SCS form in or pass through the northern/central part and their tracks are mainly westward or northwestward (e.g., Wang and Chan, 2002; Chan, 2005).

4 Discussion

In the current study, the seasonal variability of the surface wave height and its relationship with that of the sea surface wind speed in the SCS are carefully investigated with the most up-to-date gridded altimeter data. One important implication of the current results compared with previous studies is that the wave climate in the Pacific Ocean plays an important role in the wave climate variations in the SCS. The direct observational evidence is that in all months of the year the SWH in the SCS is the largest around the LS and basically decreases southward, while the high SWH around the LS in the SCS is still smaller than that in the western Pacific Ocean and thus is quite possibly the westward extension into the SCS of the latter (Figs 3 and 4).

The second evidence can be inferred from the model results of Zhou et al. (2007) and Zong and Wu (2014). Different numerical models have been utilized in the two studies. Zhou et al. (2007) utilized the WAVEWATCH-III (Tolman, 1990), while Zong and Wu (2014) used the SWAN (Simulating Waves Nearshore) (Booij et al., 1999) model. In both numerical studies, the model domain is well west of 125°E and south of 26°N. With this model configuration, the effect of the wave climate in the western Pacific Ocean on the SCS wave climate variations is excluded and the SWH in the SCS would be only controlled by the surface wind forcing over the SCS Basin. Therefore it is easy to understand their results that the SWH maxima appear in the southern SCS during winter monsoon, while in the northern SCS during summer monsoon. The reason is that during the winter northeasterly monsoon the wind fetch length is larger in the southern SCS than in the northern SCS, while during the summer southwesterly monsoon the situation is reversed. Extending the model domain eastward to about 131°E and northward to 41°N, Li et al. (2012) derived roughly the same spatial distributions of the SWH to our

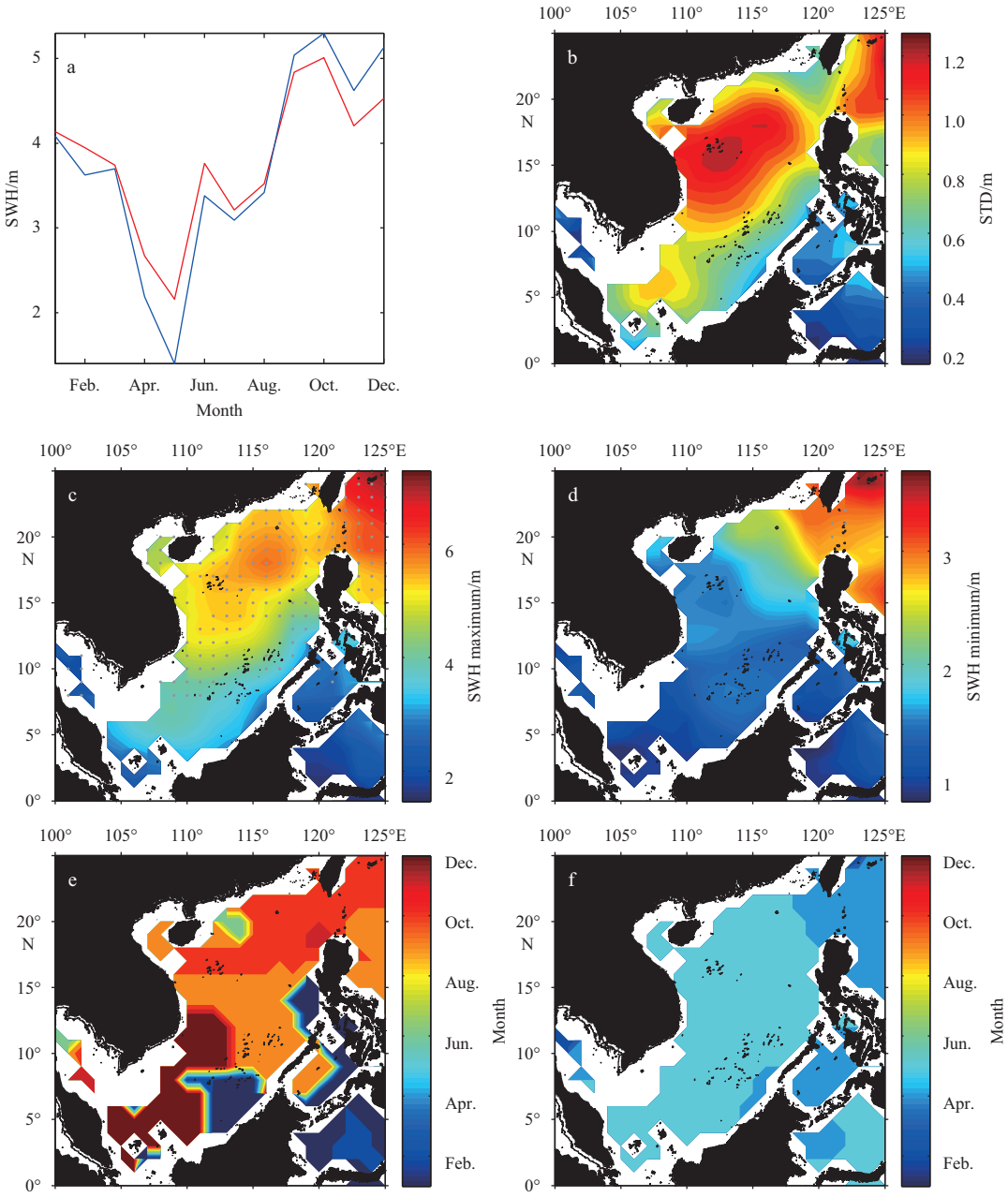

Fig. 10. Seasonality of the 99th percentile of the SWH. a. The climatological monthly SWH averaged over the whole SCS, b. the STD of the climatological monthly SWH in the SCS, c. the climatological monthly SWH maximum, d. the climatological monthly SWH minimum, e. the month when the climatological monthly SWH maximum occurs, and f. the month when the climatological monthly SWH minimum occurs.

current results in the four seasons. This, to a certain extent, proves that the wave climate in the western Pacific Ocean is quite important for the wave climate variations in the SCS, as waves generated in the Pacific Ocean can propagate into the SCS through the LS.

Third, on the basis of a series of numerical experiments with WAVEWATCH-III, Alves (2006) quantified the ocean swell contributions to the global wind-wave climate. According to his results, the ocean swells generated in the whole north Pacific Ocean could propagate into the SCS through the LS and therefore affect the wave climate in the SCS. If neglecting the surface wind forcing over the SCS, these swells would result in the similar spatial distributions of the SWH to those observed by satellites (Figs 3 and 4).

5 Summary

In this paper, the seasonal wave height variability in the SCS is investigated with the most up-to-date gridded altimeter data for the period of September 2009 to August 2015, which is merged from all available satellite missions. On average, the SWH in the SCS is the largest around the LS and then gradually decreases southwestward across the basin. As for the temporal variations, the satellite observations illustrate that the monthly time series is dominated by a significant annual cycle.

Basically, the whole SCS exhibits a uniform seasonal variation in the SWH, with the maxima occurring in December/Janu-

ary and minima in May. However, if considering the climatological seasonal means, the SWH would be weakest in summer in the northern SCS, while in spring in the central/southern SCS (Fig. 4). This is quite possibly because in the central/southern SCS the surface wind speed during the summer southwesterly monsoon is larger than that in spring and autumn, and thus results in larger wave heights of both wind sea and swell (Fig. 8). As regards the spatial distribution, the observed SWH in the SCS is the largest around the LS and then gradually decreases southward across the basin throughout the year.

The SWH generally shows consistent temporal variation on the seasonal time scale with the surface wind speed. However, the two variables have different spatial distributions in most months of the year. The most significant difference appears in summer, when the SWH is the largest around the LS and decreases southwestward across the basin (Fig. 4b), while the surface wind speed is the largest in the central SCS (Fig. 5b). All of these indicate that both swell and wind sea make important contributions to the observed wave height variations. Then the wave heights of the swell and the wind sea are separated according to the method proposed by Chen et al. (2002) and their seasonal variations are examined. The result indicates that the swell height is generally larger than the wind sea height throughout the year, and both of them are the largest in winter for the whole SCS, while weakest in summer in the northern SCS and in spring in the central/southern SCS (Figs 8a–d).

At last, the seasonal variation of the extreme wave condition in the SCS, which has been rarely studied before, is examined. During the whole period, the 99th percentile of the SWH exhibits a significant spatial variation, being large (>4.4 m) along a band extending from northwest of Luzon Island to northeast of Vietnam coast, and then decreasing both northward and southward. Its maximum value is about 4.9 m and appears around (17.5°–18.5°N, 115°–118°E). As for the seasonal variation, the 99th percentile SWH calculated with all grid points in the SCS is the largest in October and the smallest in May (Fig. 10a). A large region centering around (16°N, 112°E) in the northern SCS shows the the largest seasonal variation in the 99th percentile of the SWH (Fig. 10b), where the the largest STD of the climatological monthly 99th percentile SWH can be as high as 1.3 m. Generally, both maxima and minima of the climatological monthly SWH at the 99th percentile in the SCS decrease southward. The maxima of the climatological monthly 99th percentile SWH mainly appear in August-November in most regions of the northern and central SCS and in December/January in the southern SCS, while the minima mainly appear in May. As the mean surface wind speed is smaller in autumn than in winter, the climatological annual maxima of the 99th percentile of the SWH in the northern/central SCS is obviously associated with the TC activities.

In conclusion, though the general characteristics of the seasonal variations of the wave climate in the SCS have been extensively described with observations, model hindcasts, and wave reanalysis products, the exact dynamics at work is still unknown. As discussed in Section 4, the sea surface winds both inside and outside the SCS play quite important roles in controlling the seasonal wave climate variations in the SCS. But their exact contributions should be further quantified. Moreover, the LS should also play an important role. Besides, there are still many other questions to be resolved, such as the role played by the spatial variation of water depth in the SCS, dynamics controlling the interannual-to-decadal wave climate variations, and so on. All of these would be further investigated through high resolution numerical experiments and beyond our current scope.

References

Alves J H G M. 2006. Numerical modeling of ocean swell contributions to the global wind-wave climate. Ocean Modell, 11(1–2): 98–122

Anoop T R, Kumar V S, Shanas P R, et al. 2015. Surface wave climatology and its variability in the North Indian Ocean based on ERA-interim reanalysis. J Atmos Oceanic Technol, 32(7): 1372–1385

Booij N, Ris R C, Holthuijsen L H. 1999. A third-generation wave model for coastal regions: 1. Model description and validation. J Geophys Res, 104(C4): 7649–7666

Chan J C L. 2005. Interannual and interdecadal variations of tropical cyclone activity over the western North Pacific. Meteor Atmos Phys, 89(1–4): 143–152

Chen Qili. 1987. The South China Sea wave climate and some problems about its forecast. Mar Forecast (in Chinese), 4(2): 39–46

Chen Ge, Chapron B, Ezraty R, et al. 2002. A global view of swell and wind sea climate in the ocean by satellite altimeter and scatterometer. J Atmos Oceanic Technol, 19(11): 1849–1859

Chen Hongxia, Hua Feng, Yuan Yeli. 2006. Seasonal characteristics and temporal variations of ocean wave in the Chinese offshore waters and adjacent sea areas. Adv Mar Sci (in Chinese), 24(4): 407–415

Chia H H, Ropelewski C F. 2002. The interannual variability in the genesis location of tropical cyclones in the Northwest Pacific. J Climate, 15(20): 2934–2944

Chu P C, Qi Yiquan, Chen Yuchun, et al. 2004. South China Sea wind-wave characteristics: Part I. Validation of wavewatch-III using TOPEX/Poseidon data. . J Atmos Oceanic Technol, 21(11): 1718–1733

Dee D P, Uppala S M, Simmons A J, et al. 2011. The ERA-Interim reanalysis: configuration and performance of the data assimilation system. Quart J Roy Meteor Soc, 137(656): 553–597, doi: 10.1002/qj.828

Ewing J A, Laing A K. 1987. Directional spectra of seas near full development. J Phys Oceanogr, 17(10): 1696–1706

Fan Yalin, Lin S J, Held I M, et al. 2012. Global ocean surface wave simulation using a coupled atmosphere-wave model. J Climate, 25(18): 6233–6252

Fang Wendong, Fang Guohong, Shi Ping, et al. 2002. Seasonal structures of upper layer circulation in the southern South China Sea from in situ observations. J Geophys Res, 107(C11): 23–1, doi: 10.1029/2002JC001343

Gulev S K, Grigorieva V, Sterl A, et al. 2003. Assessment of the reliability of wave observations from voluntary observing ships: insights from the validation of a global wind wave climatology based on voluntary observing ship data. J Geophys Res, 108(C7): 3236, doi: 10.1029/2002JC001437

Guo Suiping, Zhuang Hui, Zheng Chongwei, et al. 2012. The relationship between El Niño and wave field in the South China Sea. Mar Forecast (in Chinese), 29(6): 37–43

Ha K J, Heo K Y, Lee S S, et al. 2012. Variability in the East Asian Monsoon: a review. Meteor Appl, 19(2): 200–215

Hanley K E, Belcher S E, Sullivan P P. 2010. A global climatology of wind-wave interaction. J Phys Oceanogr, 40(6): 1263–1282

Hasselmann S, Hasselmann K, Bauer E, et al. 1988. The WAM model: A third generation ocean wave prediction model. J Phys Oceanogr, 18: 1775–1810

Izaguirre C, Méndez F J, Menéndez M, et al. 2011. Global extreme wave height variability based on satellite data. Geophys Res Lett, 38(10): L10607, doi: 10.1029/2011GL047302

Jiang Haoyu, Chen Ge. 2013. A global view on the swell and wind sea climate by the *Jason-1* mission: a revisit. J Atmos Oceanic Technol, 30(8): 1833–1841

Li Chongyin. 1988. Actions of typhoons over the western Pacific (including the South China Sea) and El Niño. Adv Atmos Sci, 5(1): 107–115

Li Xunqiang, Zheng Chongwei, Su Qin, et al. 2012. Wave climate and wind climate analysis in the China Sea from 1988 to 2009. Period Ocean Univ China (in Chinese), 42(S): 1–9

Liu K S, Chan J C L. 2003. Climatological characteristics and seasonal

forecasting of tropical cyclones making landfall along the South China coast. Mon Wea Rev, 131(8): 1650–1662
Liu Qinyu, Kaneko A, Su Jilan. 2008. Recent progress in studies of the South China Sea circulation. J Oceanogr, 64(5): 753–762
Pierson Jr W J. 1991. Comment on "effects of sea maturity on satellite altimeter measurements" by Roman E. Glazman and Stuart H. Pilorz. J Geophys Res, 96(C3): 4973–4977
Pierson Jr W J, Moskowitz L. 1964. A proposed spectral form for fully developed wind seas based on the similarity theory of S. A. Kitaigorodskii. J Geophys Res, 69(24): 5181–5190
Qi Yiquan, Shi Ping. 1999. Analysis on monthly average distribution characteristics of sea surface wind and wave in South China Sea using altimetric data. Trop Oceanol (in Chinese), 18(2): 90–96
Qi Yiquan, Shi Ping, Mao Qinwen. 1997. The satellite remote sensing analysis of seasonal average characteristics of wind field and wave field in South China Sea. China Offs Plat (in Chinese), 12(3): 118–122
Sasaki W, Iwasaki S I, Matsuura T, et al. 2005. Recent increase in summertime extreme wave heights in the western North Pacific. Geophys Res Lett, 32(15): L15607, doi: 10.1029/2005GL023722
Semedo A, Sušelj K, Rutgersson A, et al. 2011. A global view on the wind sea and swell climate and variability from ERA-40. J Climate, 24(5): 1461–1479
Shanas P R, Kumar V S. 2015. Trends in surface wind speed and significant wave height as revealed by ERA-Interim wind wave hindcast in the Central Bay of Bengal. Int J Climatol, 35(9): 2654–2663
Sverdrup H U, Munk W H. 1947. Wind, sea and swell. Theory of Relations for Forecasting. Washington DC: U. S. Navy Hydrographic Office Publication 601, 50
Tao S Y, Chen L X. 1987. A review of recent research of the East Asian summer monsoon in China. In: Chang C P, Krishnamurti T N, eds. Monsoon Meteorology. New York: Oxford University Press, 60–92
Tolman H L. 1990. A third-generation model for wind waves on slowly varying, unsteady, and inhomogeneous depths and currents. J Phys Oceanogr, 21(6): 782–797
Uppala S M, Kållberg P W, Simmons A J, et al. 2005. The ERA-40 reanalysis. Quart J Roy Meteor Soc, 131(612): 2961–3012
Wan Yong, Zhang Jie, Meng Junmin, et al. 2015. A wave energy resource assessment in the China's seas based on multi-satellite merged radar altimeter data. Acta Oceanol Sin, 34(3): 115–124
Wang Bin, Chan J C L. 2002. How strong ENSO events affect Tropical Storm activity over the western North Pacific. J Climate, 15(13): 1643–1658
Wang Lei, Fung C H, Lau L K. 2007. The upper ocean thermal structure and the genesis locations of tropical cyclones in the South China Sea. J Ocean Univ China, 6(2): 125–131
Wu Lingli, Wang X L, Feng Yang. 2014. Historical wave height trends in the South and East China Seas, 1911-2010. J Geophys Res, 119(7): 4399–4409
Xie Shangping, Xie Qiang, Wang Dongxiao, et al. 2003. Summer upwelling in the South China Sea and its role in regional climate variations. J Geophys Res, 108(C8): 3261, doi: 10.1029/2003JC001867
Yu Mugeng. 1984. Analysing the characteristics of wave distribution in the South China Sea on the basis of ship reports. Mar Sci Bull (in Chinese), 3(4): 1–8
Zhai Fangguo, Wang Qingye, Wang Fujun, et al. 2014. Variation of the North Equatorial Current, Mindanao Current, and Kuroshio Current in a high-resolution data assimilation during 2008-2012. Adv Atmos Sci, 31(6): 1445–1459, doi: 10.1007/s00376-014-3241-1
Zhang Jie, Wang Weili, Guan Changlong. 2011. Analysis of the global swell distributions using ECMWF re-analyses wind wave data. J Ocean Univ China, 10(4): 325–330
Zheng Chongwei, Li Chongyin. 2015. Variation of the wave energy and significant wave height in the China Sea and adjacent waters. Renew Sust Energy Rev, 43: 381–387
Zheng Chongwei, Liu Tiejun, Qian Yuehai. 2014. The relationship between sea surface wind field, wave field and El Niño in the China Sea. J Yunnan Univ (in Chinese), 36(2): 214–223
Zheng Chongwei, Zhou Lin. 2012. Wave climate and wave energy analysis of the South China Sea in recent 10 years. Acta Energ Solar Sin (in Chinese), 33(8): 1349–1356
Zhou Liangming, Wu Lunyu, Guo Peifang, et al. 2007. Simulation and study of wave in South China Sea using WAVEWATCH-III. J Trop Oceanogr (in Chinese), 26(5): 1–8
Zhu Geli, Lin Wantao, Zhao Sen, et al. 2015. Spatial and temporal variation characteristics of ocean waves in the South China Sea during the boreal winter. Acta Oceanol Sin, 34(1): 23–28
Zong Fangyi, Wu Kejian. 2014. Research on distributions and variations of wave energy in South China Sea based on recent 20 years' wave simulation results using SWAN wave model. Trans Oceanol Limnol (in Chinese), (3): 1–12